International Journal of Fracture **105:** 161–186, 2000.

Three-dimensional numerical simulation of the Kalthoff experiment

R.C. BATRA and M.V.S. RAVINSANKAR
Department of Engineering Science and Mechanics, MC 0219, Virginia Polytechnic Institute and State University, Blacksburg, VA 24061, U.S.A.

Received 21 September 1999; accepted in revised form 18 February 2000

Abstract. We use the finite element code DYNA3D to analyze large thermomechanical deformations of a prenotched plate impacted on the notched side by a cylindrical projectile moving parallel to the axis of the notch. Both the projectile and the plate are assumed to be made of the same thermally softening but strain and strain-rate hardening material. It is found that the maximum speed imparted to points of the plate on the impact surface equals nearly 90% of the projectile speed, and the rise time depends upon the quasistatic yield stress of the material. Whereas deformations on the midsurface of the plate closely resemble a plane strain state of deformation, those on the traction free front and back surfaces are quite different. Thus measurements made on these surfaces may not describe well the deformations occurring in the interior of the plate.

Key words: Thermomechanical deformations, numerical simulation, prenotched plate.

1. Introduction

Kalthoff (1987) and Kalthoff and Winkler (1987) tested prenotched plates made of a C-300 maraging steel and impacted on the notched side by a cylindrical projectile made of the same material as the plate and moving at velocity $\mathbf{V}_0$ parallel to the axis of the notch. For a fixed radius of the notch-tip, they found that at low impact speeds the material failed due to the initiation of a crack from a point on the upper surface of the notch that is farther from the impacted edge; the straight line passing through the point and the center of the notch made an angle of approximately 70° counterclockwise with the notch-axis. However, at higher impact speeds, a shear band initiated from a point on the lower surface of the notch-tip and propagated at an angle of 10° clockwise from the axis of the notch, i.e., towards the impacted part of the plate. Kalthoff and Winkler (1987) listed the Rockwell hardness of the steel tested and Kalthoff (2000) has estimated the yield strength of this steel to be 2.1 GPa. A similar experimental set up has been employed by Mason et al. (1994) and Zhou et al. (1996a). For the impact speeds and the notch-tip radius used, only a shear band initiated from a point on the notch surface, propagated into the plate, got arrested and then a crack initiated from the shear band tip. Zhou et al. (1996a) measured the time history of the temperature at several points on the front surface of the plate and located ahead of the notch-tip. They attributed the discrepancy between their and Kalthoff's results to the difference in material properties in the two steels tested. Mason et al. (1998) have recently reported that the lowest impact speed that results in the initiation of a shear band depends upon the strength of the material characterized by its yield stress in a quasistatic simple tension or compression test.

We note that the ratio of the plate thickness to its width equals 0.0635. However, all of the numerical and analytical simulations to date (e.g., see Zhou et al., 1996b; Needleman and

Tvergaard, 1995; Batra and Nechitailo, 1997; Batra and Gummalla, 2000; Lee and Freund, 1990) have assumed that a plane strain state of deformation prevails in the plate. In the interpretation of experimental results, Mason et al. (1994) assumed a plane stress state of deformation in the plate. Chen and Batra (1998) assumed a plane strain state of deformation in the plate, strains near a crack-tip vary as $r^{-N}, 0 < N \leqslant 1$, and the stress field away from the crack-tip is given by linear elastic fracture mechanics. Here r is the distance of a point from the crack-tip. They computed the effective plastic strain near the crack-tip as a function of the angular position ϕ and showed that the maximum effective plastic strain occurs and hence the material instability initiates at $\phi \simeq -14^\circ$ for mode-mixity, $m^e = -0.25$. This value of ϕ is close to that observed by Kalthoff (1987). Lee and Freund's (1990) analysis of the dynamically loaded precracked linear elastic plate indicates that $m^e \simeq -0.25$ till the time the dilatational wave reflected from the traction-free edge of the plate arrives at the crack-tip. Recalling that the diameter of the cylindrical projectile is about eight times the thickness of the plate, the magnitude of the velocity prescribed at the surface of the plate impacted by the projectile and the rise time of the speed can not be accurately ascertained. Whereas Zhou et al. (1996b) assumed this to equal the speed of the projectile, other investigations took it to equal one-half of the projectile's speed. Also, the state of deformation in the interior of the plate need not be the same as that on its front and back surfaces where the temperature and/or deformations are measured in experiments. A three-dimensional simulation of the problem should help answer the following questions: (i) magnitude of the velocity imparted to the plate particles on the impacted surface, (ii) its rise time, (iii) where in the plate a failure initiates first, and (iv) whether or not deformations in the plate correspond to those of plane stress or plane strain. The reader is referred to a recent issue of this journal edited by Batra et al. (2000) for additional references and historical development of the failure mode transition. To the authors knowledge this is the first three-dimensional analysis of the problem.

Here, we numerically analyze three-dimensional thermomechanical deformations of the prenotched steel plate and the striker. It is found that, for the three steels studied, the maximum magnitude of the velocity imparted to the particles on the impacted face equals nearly 90% of the speed of the projectile. For the mild steel studied, the triaxiality factor at the notch-tip on the mid-plane of the plate during the first 30 μs after impact, is significantly higher than that on the front and back faces of the plate. Whereas deformations on the midplane of the plate are K_{II} dominated, those on the front and back faces of the plate have a significant K_{III} component. Results also have been computed for the case when the plate particles are constrained from moving in the thickness direction but those of the projectile can move freely. The maximum speed of the plate particles on the impact face is again found to equal approximately 90% of the speed of the projectile. The dilatational wave reaches the notch-tip at about 8 μs. The computed triaxiality factor is independent of the strength (i.e., the yield stress in a quasistatic simple tension or compression test) of the plate material until approximately 13 μs. However, subsequent values of the triaxiality factor strongly depend upon the material's strength. The deformations of the central three quarters of the plate closely resemble those computed by the plane strain assumption.

2. Formulation of the problem

A sketch of the problem studied is shown in Fig. 1. We use rectangular Cartesian coordinates and the referential description of motion to describe the locally adiabatic thermomechanical

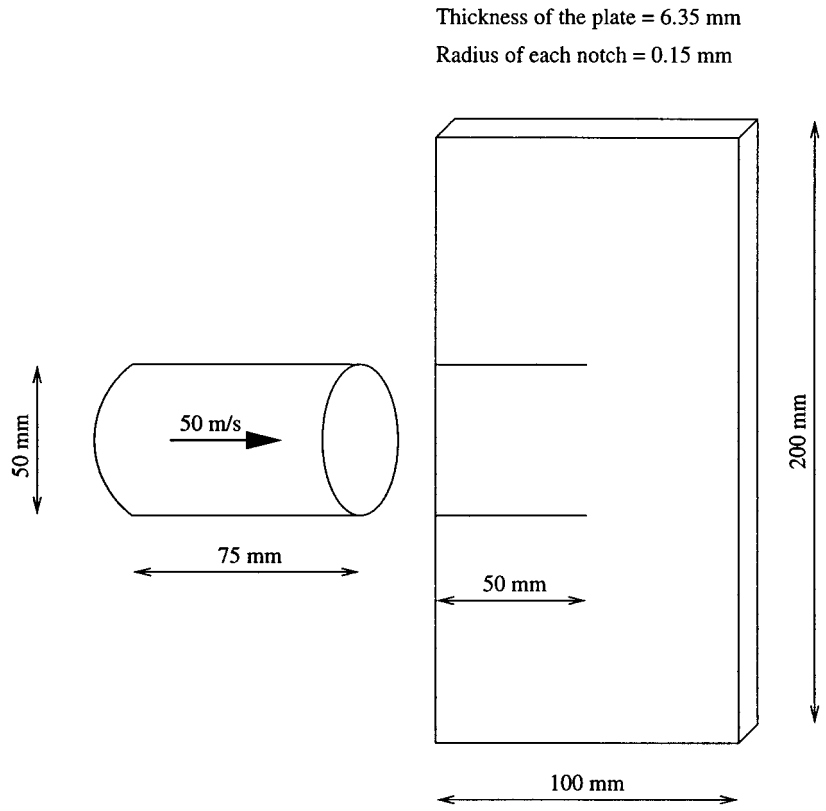

Figure 1. A sketch of the problem studied

deformations of the prenotched plate and the projectile; both are made of the same steel which is modeled as a thermally softening but strain and strain-rate hardening, isotropic and homogeneous material. In one-dimensional simulation of the initiation and the development of a shear band in a heat-conducting visco-plastic solid, Batra and Kim (1991) found that the thermal conductivity had a negligible effect on the time of initiation of a shear band but influenced the post-localization deformations of the material in the shear-banded region. Here the post-localization response of the material within a shear band has not been scrutinized because of the excessive distortions of the finite element mesh in the vicinity of the region where deformations have localized.

In the absence of body forces and external sources of energy, the balance of mass, linear momentum, moment of momentum and internal energy are

$$\rho J = \rho_o, \quad \rho_o \dot{\mathbf{v}} = \mathrm{Div}\mathbf{T}, \quad \mathbf{T}\mathbf{F}^T = \mathbf{F}\mathbf{T}^T, \quad \rho_0 \dot{e} = tr(\mathbf{T}\dot{\mathbf{F}}^T). \tag{1}$$

Here ρ is the present mass density of a material particle whose mass density in the stress-free reference configuration is ρ_0, $J = \det \mathbf{F}$, $\mathbf{F} = \mathrm{Grad}\mathbf{x}(\mathbf{X}, t)$ is the deformation gradient, Grad and Div are, respectively, the gradient and divergence operators with respect to coordinates in the reference configuration, and $\mathbf{x}$ denotes the position vector at time t of the material particle that occupied place $\mathbf{X}$ in the reference configuration. Furthermore, $\mathbf{v} = \dot{\mathbf{x}}$ is the velocity of a material particle, a superimposed dot indicates the material time derivative, $\mathbf{T}$ is the first Piola–Kirchhoff stress tensor, $\mathbf{F}^T$ equals the transpose of $\mathbf{F}$, e is the specific internal energy, and tr is the trace operator. We presume that

$$\mathbf{D} = \tfrac{1}{2}(\dot{\mathbf{F}}\mathbf{F}^{-1} + \mathbf{F}^{-T}\dot{\mathbf{F}}^{T}) = \mathbf{D}^{e} + \mathbf{D}^{p} + \mathbf{D}^{\theta},\ \mathbf{D}^{\theta} = \alpha\dot{\theta}\mathbf{1}. \tag{2}$$

and that $\mathbf{D}^{e}$, $\mathbf{D}^{p}$ and $\mathbf{D}^{\theta}$ are frame-indifferent. That is, the strain-rate tensor $\mathbf{D}$ has the additive decomposition into elastic $\mathbf{D}^{e}$, plastic $\mathbf{D}^{p}$ and thermal parts $\mathbf{D}^{\theta}$. In Equation (2), α is the coefficient of linear thermal expansion and $\mathbf{1}$ is the identity tensor.

The balance laws (1) are supplemented by the following constitutive relations.

$$\boldsymbol{\sigma} = -p\mathbf{1} + \mathbf{s}, \quad p = K(\rho/\rho_0 - 1), \quad \overset{o}{\boldsymbol{\sigma}} = \dot{\boldsymbol{\sigma}} + \mathbf{W}\boldsymbol{\sigma} - \boldsymbol{\sigma}\mathbf{W}, \tag{3}$$

$$\overset{o}{\mathbf{s}} = 2\mu\bar{\mathbf{D}}^{e}, \quad tr(\mathbf{D}^{p}) = 0, \quad \dot{e} = c\dot{\theta} + tr(\boldsymbol{\sigma}\mathbf{D}^{e} + \boldsymbol{\sigma}\mathbf{D}^{\theta})/\rho, \tag{4}$$

$$\mathbf{D}^{p} = \Lambda\mathbf{s}, \quad \sigma_{\text{eff}} = (\tfrac{3}{2}tr(\mathbf{s}\mathbf{s}^{T}))^{\frac{1}{2}}, \tag{5}$$

$$\sigma_m = (A + B(\epsilon_p)^n)(1 + C\ln(\dot{\epsilon}_p/\dot{\epsilon}_0))\left(1 - \left(\frac{\theta - \theta_0}{\theta_m - \theta_0}\right)^m\right), \tag{6}$$

where

$$\boldsymbol{\sigma} = J^{-1}\mathbf{T}\mathbf{F}^{T}, \quad \bar{\mathbf{D}} = \mathbf{D} - \tfrac{1}{3}tr(\mathbf{D})\mathbf{1}, \tag{7}$$

$$2\mathbf{W} = \text{grad}\ \mathbf{v} - (\text{grad}\ \mathbf{v})^{T}, \quad 2\mathbf{D} = \text{grad}\ \mathbf{v} + (\text{grad}\ \mathbf{v})^{T}, \tag{8}$$

$$\dot{\epsilon}_p = (\tfrac{2}{3}tr(\bar{\mathbf{D}}^{p}\bar{\mathbf{D}}^{p}))^{\frac{1}{2}}, \quad \epsilon_p = \int \dot{\epsilon}_p\, \mathrm{d}t, \tag{9}$$

$$\Lambda = 0 \quad \text{if either } \sigma_{\text{eff}} < \sigma_m \text{ or } \sigma_{\text{eff}} = \sigma_m \text{ and } tr(\mathbf{s}\overset{o}{\mathbf{s}}) \leqslant 0 \tag{10}$$

and

$$\Lambda > 0 \quad \text{if either } \sigma_{\text{eff}} > \sigma_m \text{ or } \sigma_{\text{eff}} = \sigma_m \text{ and } tr(\mathbf{s}\overset{o}{\mathbf{s}}) > 0. \tag{11}$$

Whenever Equation (11) holds, Λ is a solution of the nonlinear eqn.

$$\sigma_{\text{eff}} = \sigma_m. \tag{12}$$

Here $\boldsymbol{\sigma}$ is the Cauchy stress tensor, σ_{eff} the equivalent or the effective stress, $\mathbf{s}$ the deviatoric Cauchy stress tensor, p the pressure, K the bulk modulus, $\overset{o}{\boldsymbol{\sigma}}$ the Jaumann derivative of $\boldsymbol{\sigma}$, $\mathbf{W}$ the spin tensor, μ the shear modulus, $\mathbf{D}$ the strain-rate tensor, $\bar{\mathbf{D}}$ the deviatoric strain-rate tensor, θ the present temperature of a material particle, and *grad* the gradient operator with respect to coordinates in the present configuration. Equation $(5)_1$ states that $\mathbf{D}^{p}$ is parallel to $\mathbf{s}$, and Equation (12) is the von-Mises yield criterion with the present value of the yield stress depending on the effective plastic strain, ϵ_p, the effective plastic strain-rate, $\dot{\epsilon}_p$, and the non-dimensional temperature, $(\theta - \theta_0)/(\theta_m - \theta_0)$, where θ_0 is the reference temperature and θ_m is related to the melting temperature of the material. Equation (6) is the Johnson-Cook relation expressing the effective stress σ_m in terms of ϵ_p, $\dot{\epsilon}_p$, and θ. In Equation (6), A is the yield stress of the material in a quasistatic simple tension or compression test, parameters B and n characterize the strain hardening of the material, C and $\dot{\epsilon}_0$ the strain-rate hardening of the material, and θ_m and m the thermal softening of the material. Johnson and Cook (1983) proposed the empirical relation (6) based on torsional test data at different strain rates (all less than 500/s) and temperatures (less than 300 °C). For strain-rates ($\simeq 10^5$/s) and temperatures

(> 300 °C) likely to occur within a fully developed shear band, nearly all of the material parameters in (6) depend upon the temperature (e.g., see Klepaczko et al. (1987)). However, such dependencies have not been accounted for here for two reasons. Our study is restricted to essentially the initiation of a shear band, and there is hardly any test data available to determine these parameters as a function of the temperature. Kim and Batra (1992) considered the dependence upon the temperature of the shear modulus, thermal conductivity and the specific heat and found that the essential characteristics of the initiation and the development of a shear band are the same as for the constant values of these material parameters. The code can be modified to account for the variation of material parameters with temperature.

We note that Batra and Kim (1991) calibrated the Johnson–Cook relation (6), the power law, the Litonski relation, the Wright–Batra relation, and the Bodner–Partom law against the torsional test data of Marchand and Duffy (1988) and used them to study the pre- and post-localization response of the material deformed in simple shear. They found the values of material parameters by solving an initial-boundary-value problem and commented that the values so obtained are not necessarily unique. A defect was modeled by a nonuniform distribution of the initial temperature. Deformations of the material till the initiation of the shear band were found to be essentially independent of the constitutive relation employed, but the post-localization response considerably varied with the constitutive relation. Batra and Chen (2000) have used these constitutive relations to ascertain (i) the average strain at which a material becomes unstable, (ii) the average strain corresponding to the shear band initiation, (iii) the shear band spacing, (iv) the band width, and (v) the influence of the nominal strain-rate on the preceding quantities. The qualitative nature of the results was generally similar for the four constitutive relations studied. For the simple shearing problem, they found that the specimen size strongly influenced the band width and the energy dissipated within the band. Batra and Jayachandran (1992) used three constitutive relations to study the steady state penetration of a thermoviscoplastic target by a rigid cylindrical rod. These works suggest that the results reported herein for the Johnson–Cook relation will also be valid, at least qualitatively, for other constitutive relations until the deformations have fully localized into narrow regions.

For initial conditions, we take the prenotched plate and the projectile to be stress free and at a uniform temperature θ_0, and the plate at rest. The projectile, moving at a uniform velocity $\mathbf{V}_0$ parallel to the axis of the notch, strikes the notched edge of the plate at time $t = 0$. We take all bounding surfaces of the projectile and the prenotched plate including the notch surfaces to be thermally insulated, and all of these except for the contacting surfaces to be traction-free.

At the contact surface

$$[\mathbf{v} \cdot \mathbf{n}] = 0, \quad [\mathbf{t} \cdot \boldsymbol{\sigma}\mathbf{n}] = 0, \tag{13}$$

where $[f]$ denotes the difference in the values of f on the two sides of the contact surface, $\mathbf{n}$ is a unit outward normal to the surface, and $\mathbf{t}$ a unit vector tangent to the surface. Thus the contacting surfaces are taken to be smooth.

We note that the problem geometry and the loading conditions are symmetrical about the horizontal and vertical planes passing through the centroids of the projectile and the plate. Thus deformations of only a quarter of the domain are analyzed. The planes of symmetry are assumed to be thermally insulated, free of tangential tractions, and material particles on these planes are constrained from moving along the normal to the plane.

No fracture or failure criterion is employed, and results are computed with a fixed mesh. Thus computations were stopped when the mesh got severely distorted.

3. Computation and discussion of results

The aforestated problem is numerically analyzed by using the large scale explicit finite element code DYNA3D (Whirley and Hallquist, 1991). It uses 8-noded brick elements, one-point integration rule, an hour-glass control algorithm to eliminate spurious modes for the mechanical problem, and the conditionally stable central-difference method to integrate with respect to time t the coupled nonlinear ordinary differential equations which are the Galerkin approximation of the balance law $(1)_2$. Note that $\boldsymbol{\sigma}$ computed from Equation $(3)_3$ is symmetric. The relation $(7)_1$ then ensures that Equation $(1)_3$ is identically satisfied. Because of the referential description employed and the conservation of mass, the lumped mass matrix is evaluated only once. However, the force vector is computed after every time step first by updating the stresses. During the time interval $(t_n,\ t_{n+1})$ it is first assumed that $\mathbf{D}^e = \mathbf{D}$, stresses at time t_{n+1} are obtained from Equations (3) and (4), and Λ is computed from Equation (10) or (12). In the latter case, $\mathbf{D}^p$ is obtained from Equation $(5)_1$, and the process is repeated till the computed values of $\mathbf{D}^p$ have converged.

The constitutive relation $(4)_3$ and the balance of internal energy $(1)_4$ imply that

$$\rho c\dot{\theta} = tr(\boldsymbol{\sigma}\mathbf{D}^p). \tag{14}$$

Thus all of the plastic working rather than 90–95% of it as asserted by Taylor and Quinney (1934) is assumed to be converted into heating. Batra and Adulla (1995) showed that a smaller value of the Taylor and Quinney factor slightly delays the initiation of a shear band. Equation (14) is integrated by the central-difference method to solve for the temperature at time t_{n+1}.

The effects of thermal expansion are neglected in DYNA3D. Recalling that the plastic strain-rates depend upon the deviatoric stresses, and thermal expansion introduces hydrostatic stresses, neglecting the effects of thermal expansion will not introduce any noticeable errors in the computation of plastic deformation and hence the initiation and development of adiabatic shear bands. The points where maximum principal tensile stresses occur are not heated much because of small plastic deformations there. Thus the computed values of the maximum principal tensile stress should be reasonably accurate.

The hour-glass viscosity coefficient was set equal to 0.1 in order to suppress spurious or hour-glass modes. The time step size equaled 90% of the time taken by the dilatational wave to travel through the smallest element in the mesh. We note that the time step size decreased significantly as the mesh adjacent to the surface of the notch-tip got severely deformed.

We assume that the plate and the projectile are made of a mild steel, and assign following values to various material parameters in the computation of results.

$$\begin{aligned}
&\rho_0 = 7,850 \text{ kg m}^{-3}, \quad \mu = 76 \text{ GPa}, \quad K = 156 \text{ GPa}, \quad c = 452 \text{ J kg}^{-1}\,^{\circ}\text{C}^{-1},\\
&A = 792.2 \text{ MPa}, \quad B = 509.5 \text{ MPa}, \quad n = 0.26, \quad C = 0.014, \quad m = 1.03,\\
&\theta_m = 1033 \text{ K}, \quad \theta_0 = 25\,^{\circ}\text{C}, \quad \dot{\epsilon}_0 = 1/\text{s}.
\end{aligned} \tag{15}$$

Results reported herein are for a notch-tip radius of 0.15 mm and 50 m/s speed of the projectile. The minimum notch-tip radius used in Kalthoff's experiments equaled 0.3 mm. Values of material parameters in (15), except possibly for the value of θ_m, are for a typical steel.

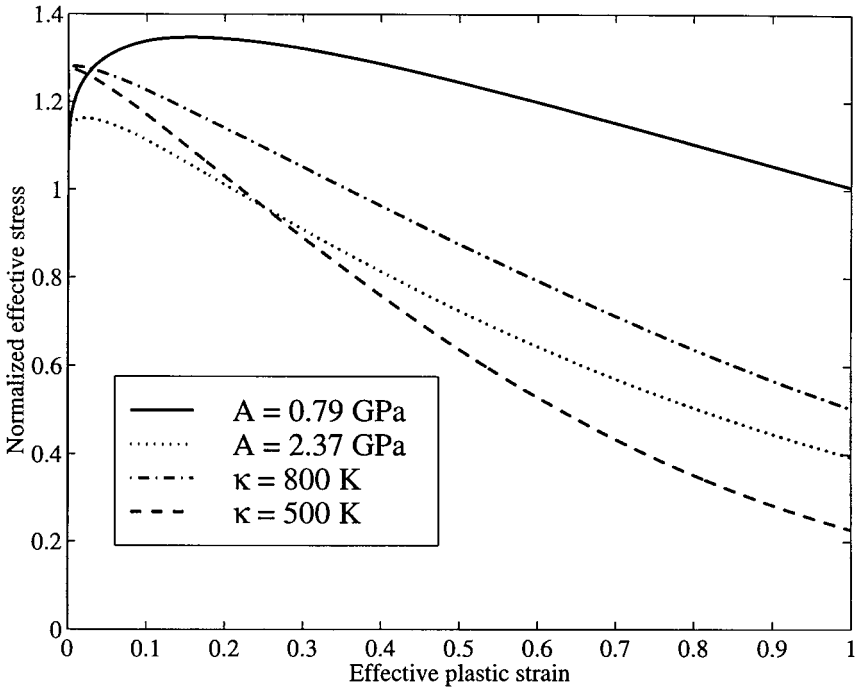

Figure 2. Effective stress vs. effective plastic strain curves for locally adiabatic homogeneous deformations of the material of the plate and the projectile at an effective strain-rate of 10^5/s.

Figure 2 depicts the effective stress vs. the effective plastic strain curve for locally adiabatic homogeneous simple shearing or plane strain deformations of the steel with values of material parameters given in (15) and deformed at an effective strain-rate of 10^5/s. The effective stress is maximum at an effective plastic strain of 0.15. Prior to this strain level, strain and strain-rate hardening of the material exceed its softening caused by the temperature rise, and subsequently the thermal softening exceeds the combined hardening effects. The other three curves included in Fig. 2 will be commented upon later.

We focus on studying the deformations of the plate material around the notch tip; thus details of the deformations of the projectile are not described here. Both the plate and the cylindrical projectile were discretized into 8-noded brick elements; the discretization of the plate region near the notch-tip in a $X_1 - X_2$ plane is exhibited in Fig. 3. It has 24 elements around the notch-tip, and the element size gradually increases with the distance from the notch-tip. For a notch-tip radius of 0.15 mm, the size of an element abutting the surface of the notch-tip equals 19.6 $\mu m \times 19.6\ \mu m$. The half-thickness of the plate was divided into 10 equal parts or layers, and $X_3 =$ constant planes passing through the centroids of the elements in these layers are called planes 1 through 10 with plane 1 being closest to the mid-plane and plane 10 nearest to the free surface of the plate. For the corresponding plane strain problem, Batra and Gummalla (2000) found that results computed with this mesh were virtually the same as those obtained by using a considerably finer mesh.

The aforestated problem was also analyzed by constraining to zero the displacements of plate particles in the thickness direction but considering three-dimensional deformations of the projectile; this is identified below as a two-dimensional (2-D) problem. Since the contact

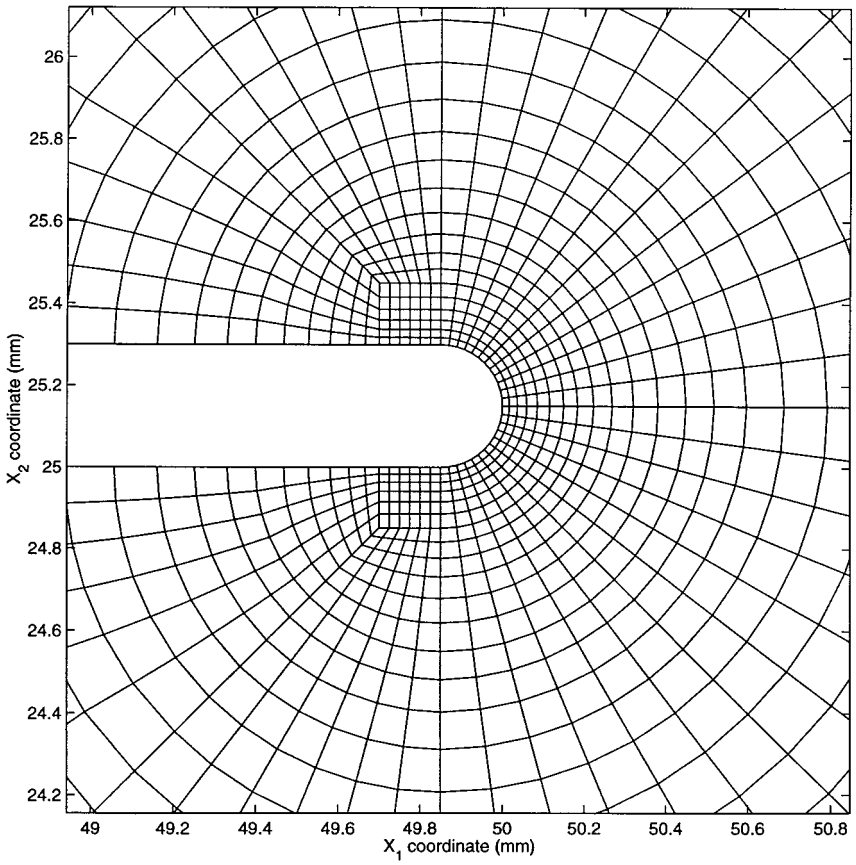

Figure 3. Finite element discretization of the region near the notch-tip in the $X_1 - X_2$ plane.

surface is smooth, there will be relative sliding between the projectile and plate particles abutting the common interface.

Figure 4 evinces, for the 3-D and 2-D problems, the time history of the normalized average x_1-velocity of all 121 nodes on the contact surface between the plate and the projectile; the normalized speed of a plate particle equals its speed divided by the initial speed (50 m/s) of the projectile. At any time, the difference between the maximum and the minimum x_1-velocity of nearly all nodes on the contact surface of the plate was less than 5% of their mean value. Thus, the time-history plotted in Fig. 4 is representative of that for any node on the contact surface. It is clear that the maximum speed imparted to a plate particle on the contact surface equals approximately 90% of the speed of the projectile. As also noted by Ravi-Chandar et al. (2000), a one-dimensional analysis of the impact between two bodies having unequal areas at the impact face reveals that the normalized x_1-velocity given to a plate particle equals $(1 + A_p/A_r)^{-1}$ where A_p and A_r are, respectively, the impacted area of the plate and the area of cross-section of the projectile. For the present problem, $(1 + A_p/A_r)^{-1} = 0.861$ so that the one-dimensional (1-D) analysis provides a good approximation of the maximum speed of plate particles on the impacted surface of the plate. However, the 1-D analysis does not give an estimate of the rise time of this speed.

At time $t = 30$ μs after impact, Figs. 5a, 5b and 5c exhibit, respectively, the fringe plots of the effective plastic strain in the projections on the $X_1 - X_2$ plane of the deformed configu-

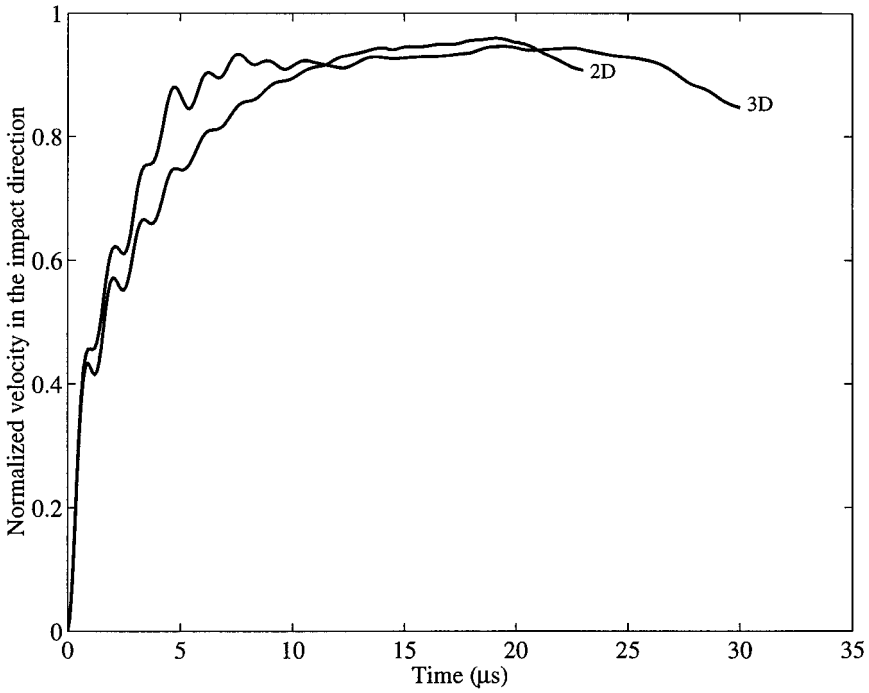

Figure 4. Time-history of the normalized average X_1-velocity of all of the 121 plate nodes on the contact surface between the plate and the projectile.

rations of layers 1, 8 and 10; Fig. 5d depicts the corresponding results for the 2-D problem at $t = 23\ \mu$s. The finite element meshes were excessively distorted at $t = 30$ and 23 μs for the 3-D and 2-D simulations respectively. The deformation patterns in layers 2 through 7 were found to be essentially similar to that in layer 1 and are omitted. Points on the midsurface, $X_3 = 0$, of the plate are constrained to stay on that plane. The plots in Figs. 5a, 5b and 5c reveal that material points near the lower surface of the notch-tip on planes $X_3 = h/20, 2h/5$ and $h/2$ move in the impact direction; here h equals the thickness of the plate. The displacement of these points in the impact direction increases rather exponentially with their distance from the midplane of the plate. Note that in each layer large values of the effective plastic strain occur in a very small region near the lower part of the notch-tip. Whereas the maximum effective plastic strain in layer 1 equals almost 100%, that in layers 8 and 10 equals approximately 95% and 65% respectively. In layer 1 between planes $X_3 = 0$ and $X_3 = h/20$, there are two narrow regions of intense plastic deformation with strains exceeding 0.2; one is aligned along the axis of the notch-tip and the other at approximately 135° clockwise from it. However, in layers 8 and 10 with layer 10 abutting the traction-free front face of the plate, there is only one thin region of large plastic deformation parallel to the axis of the notch which agrees with the test observations, made on the front face of the plate, that a shear band propagates essentially parallel to the notch-axis. Fringe plots of the effective plastic strain shown in Fig. 5d indicate that for the 2-D problem a shear band initiating from a point on the lower surface of the notch-tip has two lobes - one nearly parallel to the axis of the notch and the other at about 130° clockwise from that direction. At $t = 23\ \mu$s, the maximum effective plastic strain equals almost 120% which is higher than that found at any point in the 3-D problem till $t = 30\ \mu$s. Also, the notch-tip is more severely deformed in the 2-D problem as compared to that in the

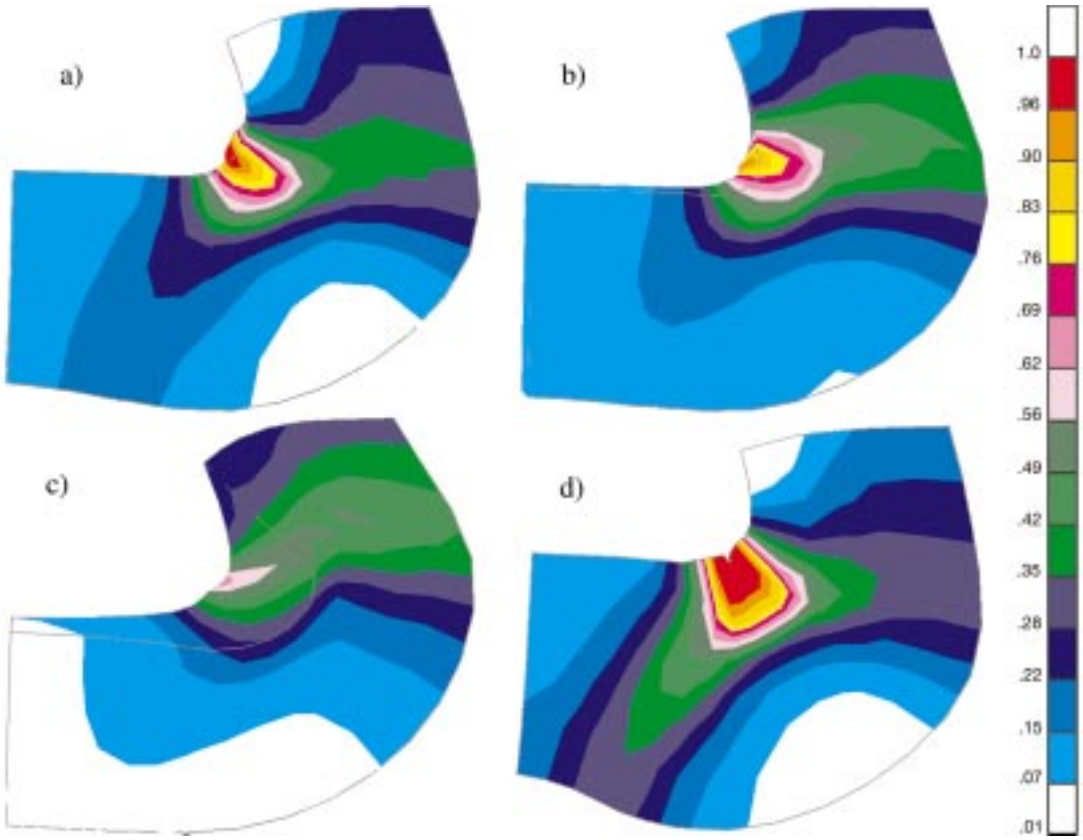

Figure 5. Fringe plots of the effective plastic strain in the projections onto the $X_1 - X_2$ plane of the deformed configurations of layers 1, 8 and 10 for the 3-D simulation and (d) the 2-D simulation.

3-D problem. These results imply that deformations near the midplane of the plate closely correspond, at least qualitatively, to those obtained by assuming that a plane strain state of deformation prevails in the plate. The values, in the two cases, of the maximum effective plastic strain at any point of the plate and the times when they occur are generally quite different.

We have plotted in Figs. 6a and 6b, for two different values of the time t, the variation of the effective plastic strain vs. the referential angular position of the centroids of elements abutting the round surface of the notch-tip. Results for elements in layers 1, 8 and 10 for the 3-D problem are identified in Fig. 6a as curves P1, P8 and P10 respectively; those for the 2-D problem are shown in Fig. 6b. Both for the 2-D and 3-D problems, elements on the notch surface in the angular region $25^\circ \leqslant \phi \leqslant 90^\circ$ have undergone intense plastic deformations; here the positive angle is measured clockwise from the notch-axis. For the 3-D problem, the angular width of the severely deformed region and the magnitude of the effective plastic strain in elements of layer 10 are quite different from their values in the corresponding elements of layers 1 and 8. As also noted above, for the 3-D problem the maximum effective plastic strain in any element of layer 10 is approximately one-half of that in the elements of layer 1. The 2-D simulations predict higher values of the maximum effective plastic strain than that obtained in the similarly located element in any of the ten layers in the 3-D simulations.

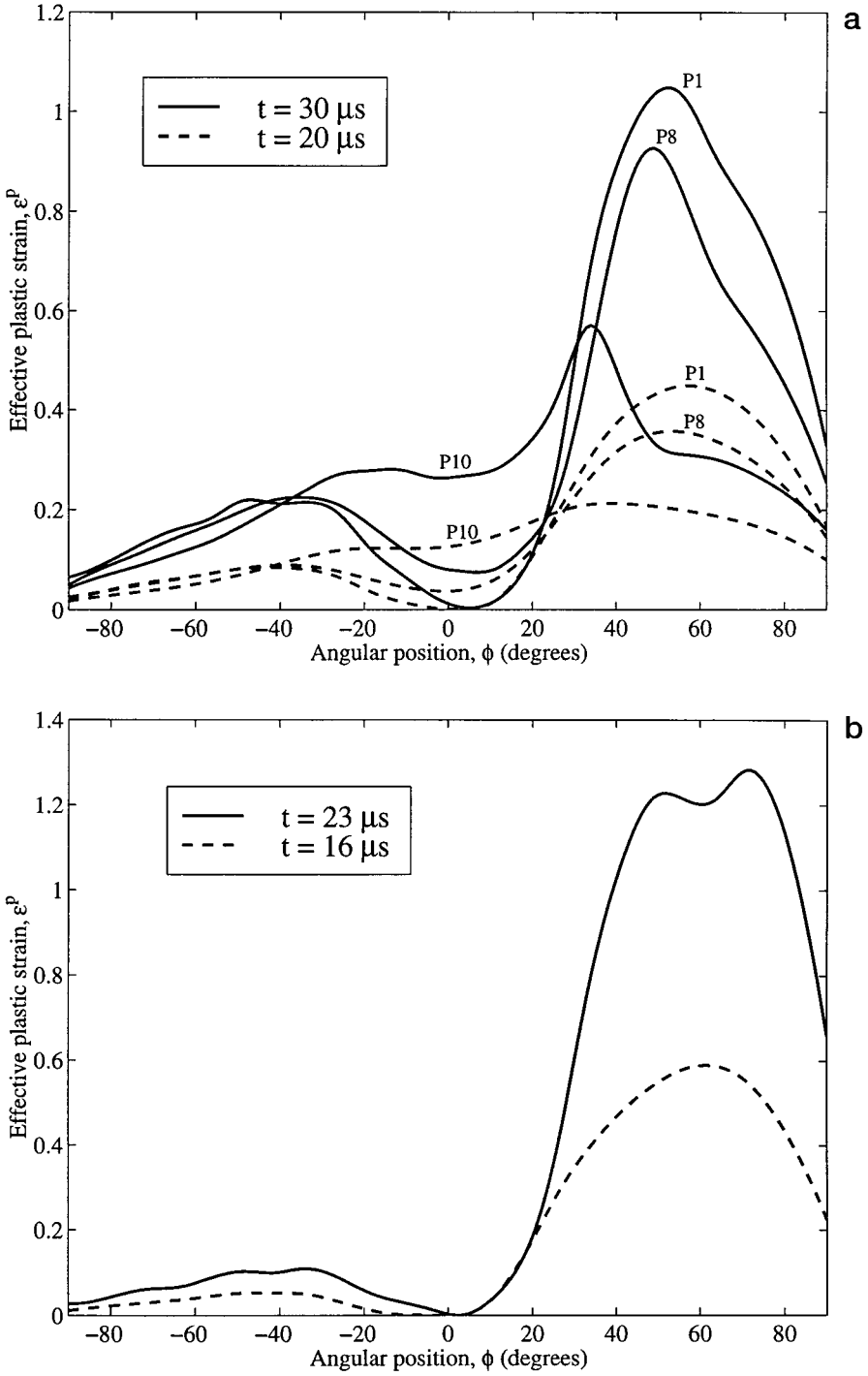

Figure 6. Distribution, at two values of the time t, of the effective plastic strain on the surfaces of the notch-tip; (a) 3-D simulation, and (b) 2-D simulation.

For the 3-D problem, Figs. 7a–d depict the time-history of the effective stress, effective plastic strain, temperature and the triaxiality factor at the material points whose referential locations with respect to cylindrical coordinates with the origin at the center of the notch-tip and on the midplane of the plate are (0.16 mm, 63.75°, $h/40$), (0.16 mm, 48.75°, $3h/8$) and (0.16 mm, 33.75°, $19h/40$). Results for these three points are signified in Figs. 7a–7d by P1, P8 and P10 respectively. Curves labeled 2D give the corresponding results for the 2-D problem at the material point that occupied the place (0.16 mm, 63.75°) in the reference configuration. Both for the 3-D and 2-D simulations, the effective stress increases rapidly soon after a loading wave arrives at the notch-tip, attains a maximum value and then gradually drops. Because of the different time histories of deformation, the peak value of the effective stress and its rate of drop vary from point to point. The effective stress drops more rapidly in the 2-D problem as compared to that at any of the three points considered in the 3-D problem. Results plotted in Fig. 7d indicate that the triaxiality factor, $-\sigma_{ii}/3\sigma_{\text{eff}}$, increases with time rather sharply for the 2-D problem. However, for the 3-D problem, the triaxiality factor increases slowly with time at the points in layers 1 and 8, and decreases slowly with time at the point in layer 10. The triaxiality factor for the 2-D simulations is much higher than that for the 3-D simulations. Vandergiessen (1995) has suggested that higher values of the triaxiality factor enhance the nucleation of voids. Thus the 2D simulations will predict an earlier failure of the material as compared to the 3D simulations. Curran et al. (1987), Tvergaard and Needleman (1984) and Perzyna (1986) have proposed that whenever $\sigma_{ii} > 0$ the stress controlled nucleation of voids depends exponentially upon $(-|\sigma_{ii} - \sigma_N|)$ where $\sigma_N > 0$ is the threshold value of the mean stress. The present simulations indicate that $\sigma_{ii} < 0$ within a shear band. Thus there will hardly be any nucleation and growth of voids due to the extreme values of the stresses. However, voids may nucleate because of the effective plastic strain exceeding a critical value. We note that the nucleation and growth of voids have not been considered in this study.

Batra and Rattazzi (1997) used the following four definitions for the initiation of a shear band at the root of a v-notch in a thick-walled steel tube: (i) the effective stress has dropped to 90% of its maximum value and the material particle is loading plastically, (ii) the effective stress has dropped to 80% of its maximum value and the material particle is loading plastically, (iii) the effective plastic strain equals 0.5, (iv) the effective plastic strain equals 1.0. Each one of the four definitions gave a different value of the time of initiation and the speed of propagation of a shear band. The definition (i) was proposed by Batra and Kim (1992) based upon the results of their numerical simulation of the simple shearing deformations of twelve materials. We note that no *in-situ* observations of the time history of the temperature, plastic strain and/or the effective stress within a shear band are available. The effective plastic strain at the initiation of a shear band depends on the shape and size of the defect (e.g., cf., Batra and Kim, 1992). In their torsional tests on thin-walled HY-100 steel tubes, Marchand and Duffy (1988) postulated that a shear band initiates when the torque required to deform the tube suddenly drops. They estimated the shear strain within a band to be 20. Mason et al. (1994) have reported an effective plastic strain of 1.0 in a shear band formed in a C-300 maraging steel plate, and Zhou et al. (1996a) have given the time histories of the temperature at a point on the front face of the prenotched plate and situated approximately 6-mm ahead of the notch-tip. In their numerical simulations of the Kalthoff experiment on a C-300 maraging steel plate, Zhou et al. (1996b) assumed that the plastic strain at the shear band tip equaled 0.17 and 0.0636 at effective plastic strain-rates of 4×10^4/s and 4×10^5/s respectively. Here we adopt the definition (i) for the initiation of a shear band because it incorporates the primary characteristic that the effective stress drops within a shear band. The shape and size of the

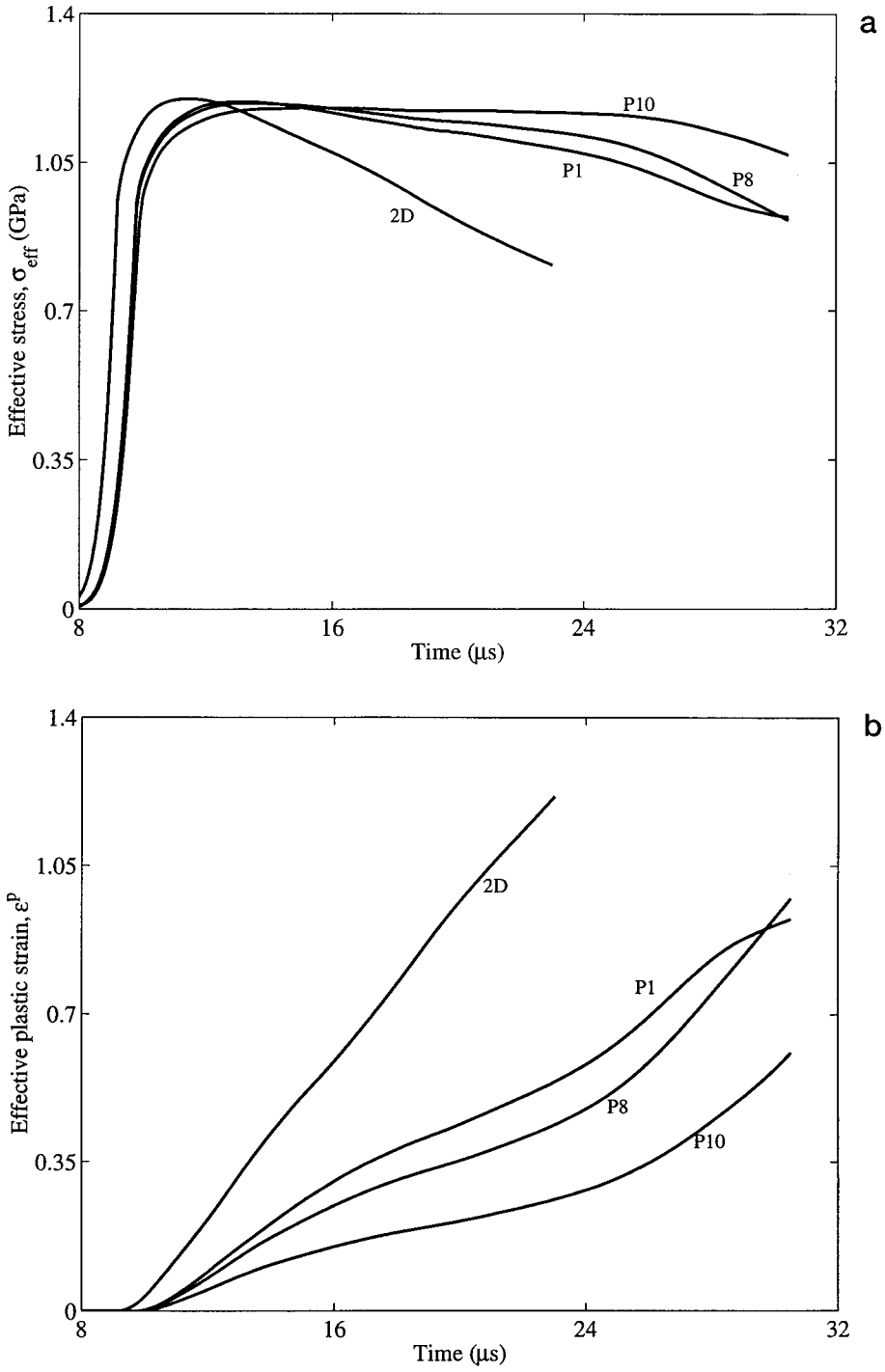

Figure 7. Time-history of the (a) effective stress, (b) effective plastic strain, (c) temperature and (d) the triaxiality factor at a material point near the lower surface of the notch-tip in planes 1, 8 and 10 for the 3-D simulation and at a similarly situated point for the 2-D simulation.

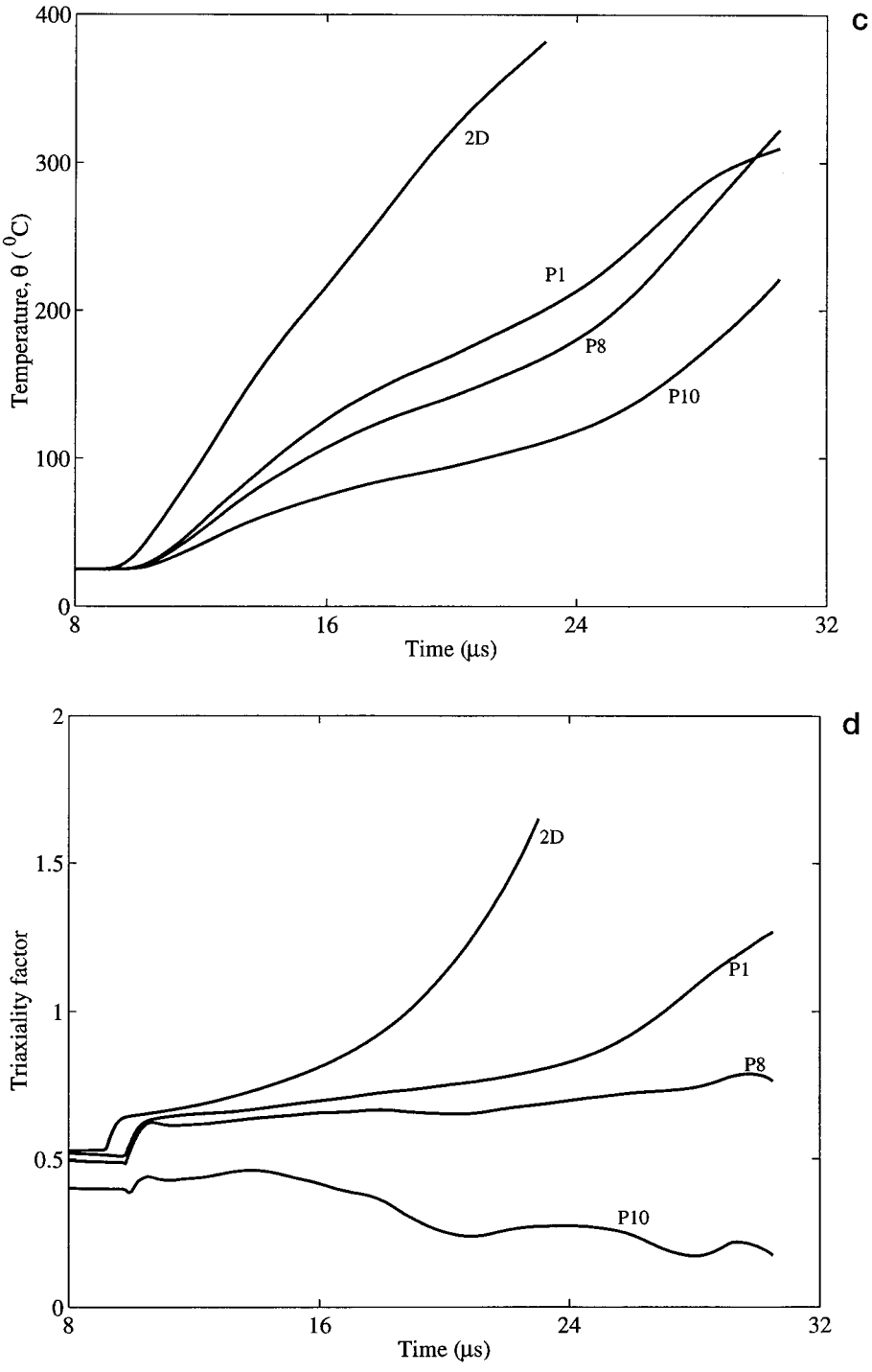

Figure 7. Continued.

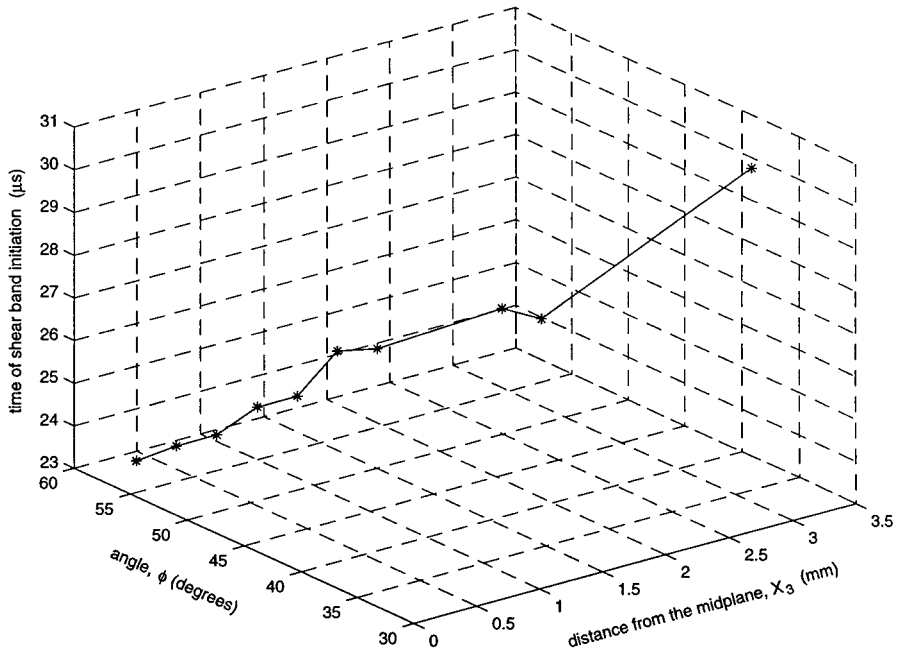

Figure 8. Time of initiation of a shear band and where it initiates first at points around the lower surface of the notch-tip.

defect is also tacitly accounted for, albeit approximately. The exact value of the effective plastic strain at the shear band tip will depend upon the material, the loading conditions and the shape and size of defect; thus adopting universal values of 0.5 or 1.0 may not be very realistic. Similarly, a relation between ϵ_p and $\dot{\epsilon}_p$ at the instant of the initiation of a shear band may not account for the shape and the size of the defect, and may result in the initiation of a shear band even before the effective stress has attained its maximum value.

Our definition of the initiation of a shear band implies that it initiates at the points in layers 1, 8 and 10 at time $t = 24$, 26.2 and 30.5 μs respectively for the 3-D simulations, and at time $t = 15.8$ μs for the 2-D simulation. The effective plastic strain and the temperature rise at the instant of the initiation of a shear band at these points equal (0.58, 188 °C), (0.6, 193 °C), (0.61, 196 °C) and (0.57, 186 °C), respectively. These values of temperature rise compare favorably with 227 °C measured by Zhou et al. (1996a) in a C-300 maraging steel and 200 °C by Marchand and Duffy (1988) in a HY-100 steel. Results plotted in Fig. 21 of Marchand and Duffy (1988), in Fig. 8 of Zhou et al. (1996a) and in Fig. 10 of Batra and Kim's (1990) paper indicate that both in the experiments and numerical simulations, the temperature rises sharply within the shear banded region after the deformations have started to localize. It is evident that a shear band first initiates at a point on the midplane and then at the points in layers 8 and 10.

According to any one of the aforestated criteria for the initiation of a shear band, it initiates sooner in the 2-D simulations as compared to that in the 3-D simulations. Using criterion (i) for the initiation of a shear band, knowing the distance between planes 1 and 8, and by computing the time elapsed between the initiations of shear bands on these two planes, we find the average speed of a shear band in the thickness direction to be 1155 m/s. The aforestated four definitions of the initiation of a shear band give quite different results. For example, according to definition (i) a shear band has not initiated at a point on plane 10 till $t = 30.5$ μs,

but according to definition (iii) it initiated there at $t = 29$ μs. We note that plane 10 is close to the traction-free bounding surface of the plate, and plane 1 is adjacent to the mid-surface of the plate.

The 3-dimensional plot in Fig. 8 shows the time of initiation and where around the notch-tip a shear band initiates first in each of the ten layers. It is clear that the angular position, 34°, of the point of initiation of a shear band in the layer abutting the front face of the plate is different from the approximately 64° location in layers 1 through 7. As the shear band propagates from the midsurface to the front face of the plate, its speed decreases; it propagates much slower from layer 9 to layer 10 as compared to its average speed of propagation from layer 1 to layer 8. At $t = 30$ μs, the width of the shear band in layers 1, 8 and 10 equals 50 μm, 40 μm and 30 μm respectively.

In an attempt to further understand which stress components significantly contribute to the deformations of the material around the notch-tip, we have plotted in Figs. 9a–f the time-history of the six components of the Cauchy stress tensor at the same points for which results were plotted in Fig. 7. At the point in layer 1, at $t = 9$ μs, the magnitude of σ_{11} is much greater than that of σ_{22} and σ_{33}, and all of the normal stresses are compressive. However, at $t = 30$ μs, the magnitudes of σ_{11}, σ_{22} and σ_{33} are about the same and all of them are compressive. Whereas σ_{12} nearly equals σ_{22} at each one of the three points, σ_{13} and σ_{23} on plane 1 essentially vanish, and σ_{13} is quite small on planes 8 and 10. However, at the point on plane 10, the maximum value of $|\sigma_{23}|$ is about eight-tenth of the maximum value of $|\sigma_{12}|$ there. Because of the noticeable displacements in the x_3-direction of material particles on the front traction-free surface of the plate, the outward unit normal to it in the deformed configuration is no longer parallel to the x_3-axis. Thus σ_{13}, σ_{23} and σ_{33} need not vanish at points on the front surface of the plate. Recalling that plastic deformations are caused by deviatoric stresses, we conclude that initially the normal stresses and σ_{12} contribute significantly to the value of σ_{eff} at points on planes 1 through 8, but at $t = 30$ μs, only σ_{12} makes noticeable contributions to σ_{eff}. However, at the point on plane 10, s_{22} and σ_{12} cause plastic deformations of the material. Thus it may not be very realistic to assume that a plane state of stress prevails in the plate.

Figures 10a and 10b exhibit, respectively, for the 3-D and 2-D simulations the variation of the normalized maximum principal stress vs. the angular position, in the reference configuration, of the centroids of elements abutting the notch surface. A comparison of these results with those plotted in Fig. 6 reveals that the maximum principal stress is compressive in elements where the effective plastic strain is high and is tensile in less severely deformed elements which lie on the upper surface of the notch-tip. As the plastic deformations get localized in the region near the bottom of the notch-tip, the magnitude of the algebraically largest principal stress increases in elements of layer 1 but remains essentially unchanged in elements of layer 10. The angular distribution of the maximum principal stress in the 2-D simulations closely resembles that in layer 1 for the 3-D simulations. The time-history of the maximum principal stress at material points (0.37 mm, $-63.75°$, h/40) and (0.37 mm, $-63.75°$, 19h/40) in the 3-D simulations and at the material point (0.37 mm, $-63.75°$) in the 2-D simulations is exhibited in Fig. 10c. It is evident that the maximum principal tensile stress reaches a plateau at $t \simeq 18$ μs both in the 3-D and 2-D simulations. The maximum principal tensile stress in the element of layer 10 is lower than that in the element of layer 1 signifying that a brittle failure, if it occurs, will first initiate in the elements of layer 1, i.e., near the midplane of the plate. In the reference configuration, the line joining this point on the upper surface of the notch-tip to its center makes an angle of 63.75° counterclockwise with the axis of the notch. Depending upon the value of the principal tensile stress at the instant of brittle failure, the times of initiation

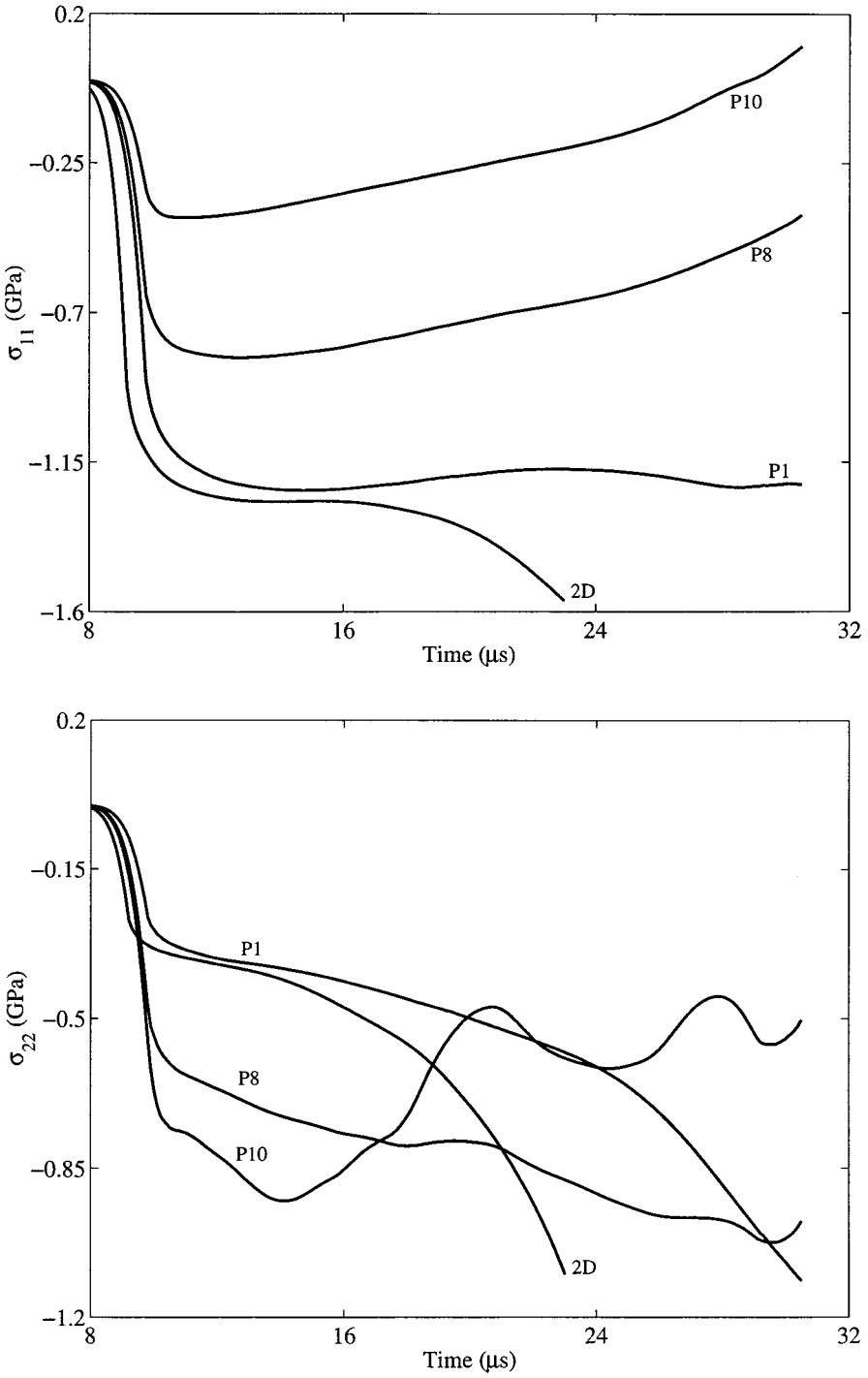

Figure 9. Time-history of the six components of the Cauchy stress tensor at points (0.16 mm, 63.75°, h/40), (0.16 mm, 48.75°, 3 h/8) and (0.16 mm, 33.75°, 19 h/40) for the 3-D simulation and at the point (0.16 mm, 63.75°) for the 2-D simulation.

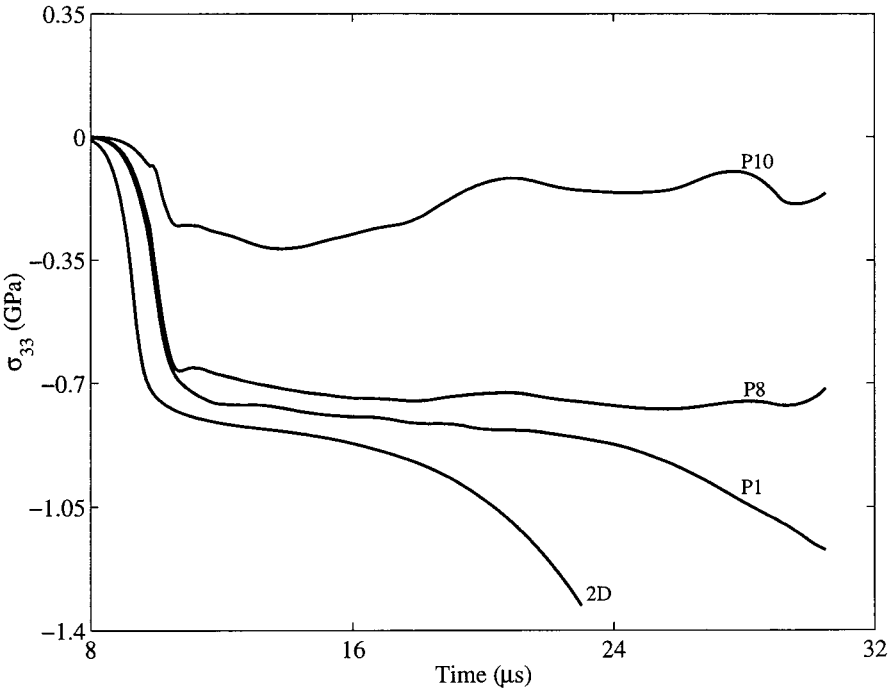

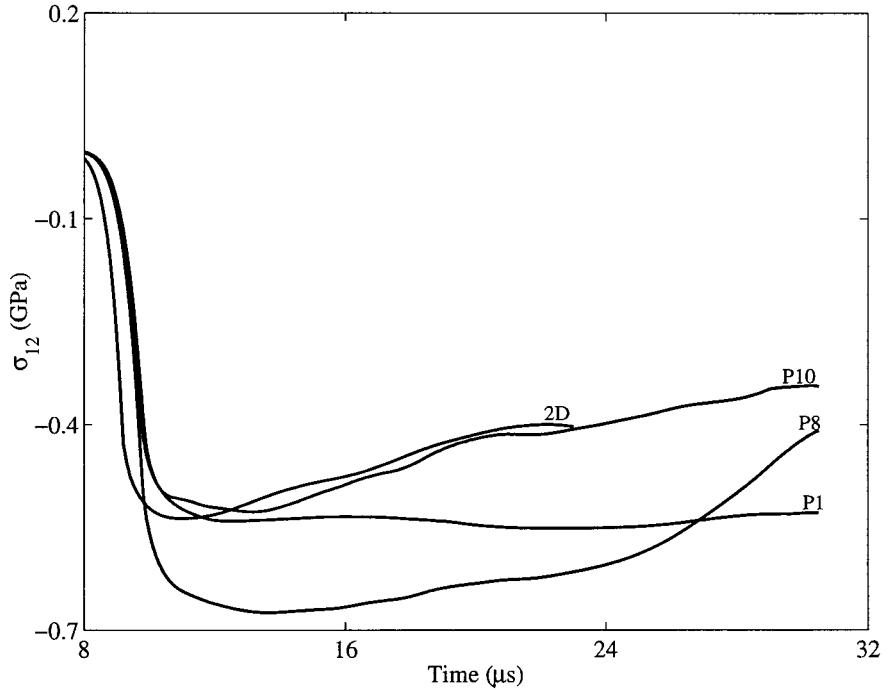

Figure 9. Continued.

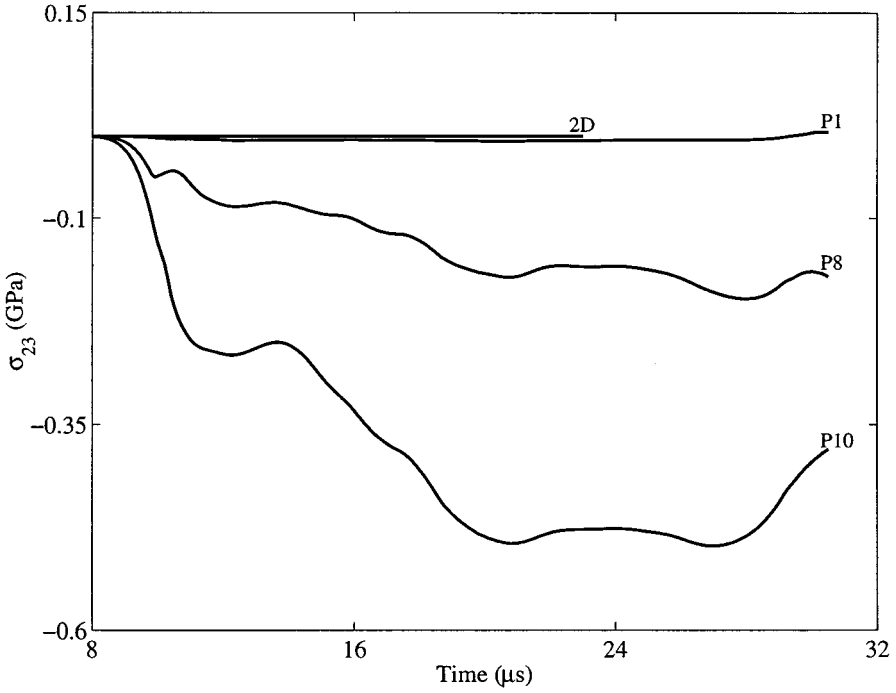

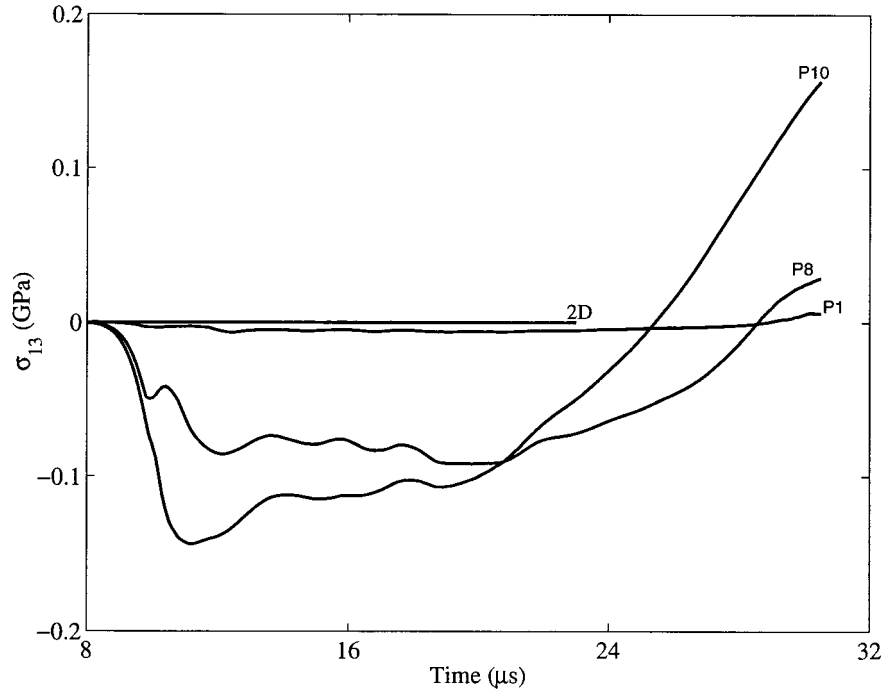

Figure 9. Continued.

of the brittle failure predicted by the 2-D and 3-D simulations will significantly differ. The values listed in Tables 5.7 and 5.2 and the results plotted in Fig. E5.2 of Dowling's (1993) book give that $(\sigma_f/\sigma_0, \epsilon_f)$ for AISI 1020HR steel, AISI 4142 steel tempered at 450 °C and 18 Ni Maraging steel equal (2.67, 1.1), (1.33, 0.66) and (1.19, 0.82) respectively. Here σ_f and ϵ_f equal, respectively, the true axial stress and the axial strain at fracture in a simple tensile test and σ_0 is the yield stress of the material. The large values of ϵ_f indicate that significant plastic deformations occurred prior to the failure of the material; this is a characteristic of the ductile rather than the brittle failure. Zhou et al. (1996b) and Batra and Gummalla (2000) assumed that σ_p/σ_0 equals respectively 3.0 and 2.0 at the instant of brittle failure; σ_p equals the tensile principal stress. Ritchie et al. (1973) have proposed that the brittle failure occurs when $\sigma_p/\sigma_0 = 3.0$ over a certain length which is characteristic of the microstructure of the material and typically equals the grain diameter. Because of the one-point integration rule used in DYNA3D, stresses within an element are assumed to be constant. Also, the smallest dimension, 16 μm, of an element probably exceeds the grain size. Assuming that the brittle failure ensues when $\sigma_p/\sigma_0 = 2.0$, for the present problem brittle failure will not occur.

We now study the effect of the material strength as represented by the quasistatic yield stress of the material. Plane strain numerical simulations of Batra and Gummalla (2000) and test observations of Roessig et al. (1998) indicate that the material strength significantly influences the onset of a shear band in the plate impact problem.

3.1. Effect of material strength

The impact problem was also analyzed by changing the value of A in (15) from 792.2 MPa to 2360 MPa and keeping unchanged the values of all other material and geometric parameters. The normalized effective stress vs. effective plastic strain curve in Fig. 2 for homogeneous simple shearing deformations of the steel at a strain-rate of 10^5/s indicates that this steel exhibits higher thermal softening as compared to the steel with $A = 792.2$ MPa. This is evidenced by the higher magnitude of $|\mathrm{d}\sigma_{\mathrm{eff}}/\mathrm{d}\epsilon_p|$ for the stronger steel. The effective stress peaks at effective plastic strains of 0.04 and 0.15 for the steels with $A = 2360$ MPa and 792.2 MPa, respectively. These observations suggest that in the Kalthoff problem, the time of initiation of a shear band will decrease with an increase in the value of A.

The time-history of the evolution of the normalized x_1-velocity of the plate particles on the projectile/plate interface revealed that, both for the 2-D and 3-D simulations, the maximum x_1-velocity of the plate particles equaled about 90% of the initial speed of the projectile. However, the normalized x_1-velocity of these plate particles increased linearly from 0 to 0.45 in 1 μs, and then affinely to 0.9 in the next 9 μs for the steel with $A = 2.36$ GPa. For the steel with $A = 0.792$ GPa, the peak in the x_1-velocity of the plate particles occurred at $t \simeq 7$ μs. As for the steel with $A = 0.792$ GPa, the deformations of elements in layers 8, 9 and 10 were found to be significantly different from those in corresponding elements of layers 1 through 7. The fringe plots of the effective plastic strain in layers 1, 8 and 10 for the 3-D simulations revealed that a shear band with two lobes of nearly equal effective plastic strain ensued in layer 1 from a point on the bottom surface of the notch-tip. However, the shear band in layers 8 and 10 had only one lobe parallel to the axis of the notch. The fringe plots in layer 1 closely matched those for the plane strain problem. The plot of the time-history of the effective stress at points abutting the notch-tip in layers 1, 8 and 10 and at the corresponding point for the 2-D problem revealed that, according to definition (i), a shear band initiated at $t = 12.5$ μs for the 2-D problem, and at $t = 13.2$, 13.4 and 14.8 μs in an element in layers 1, 8 and 10

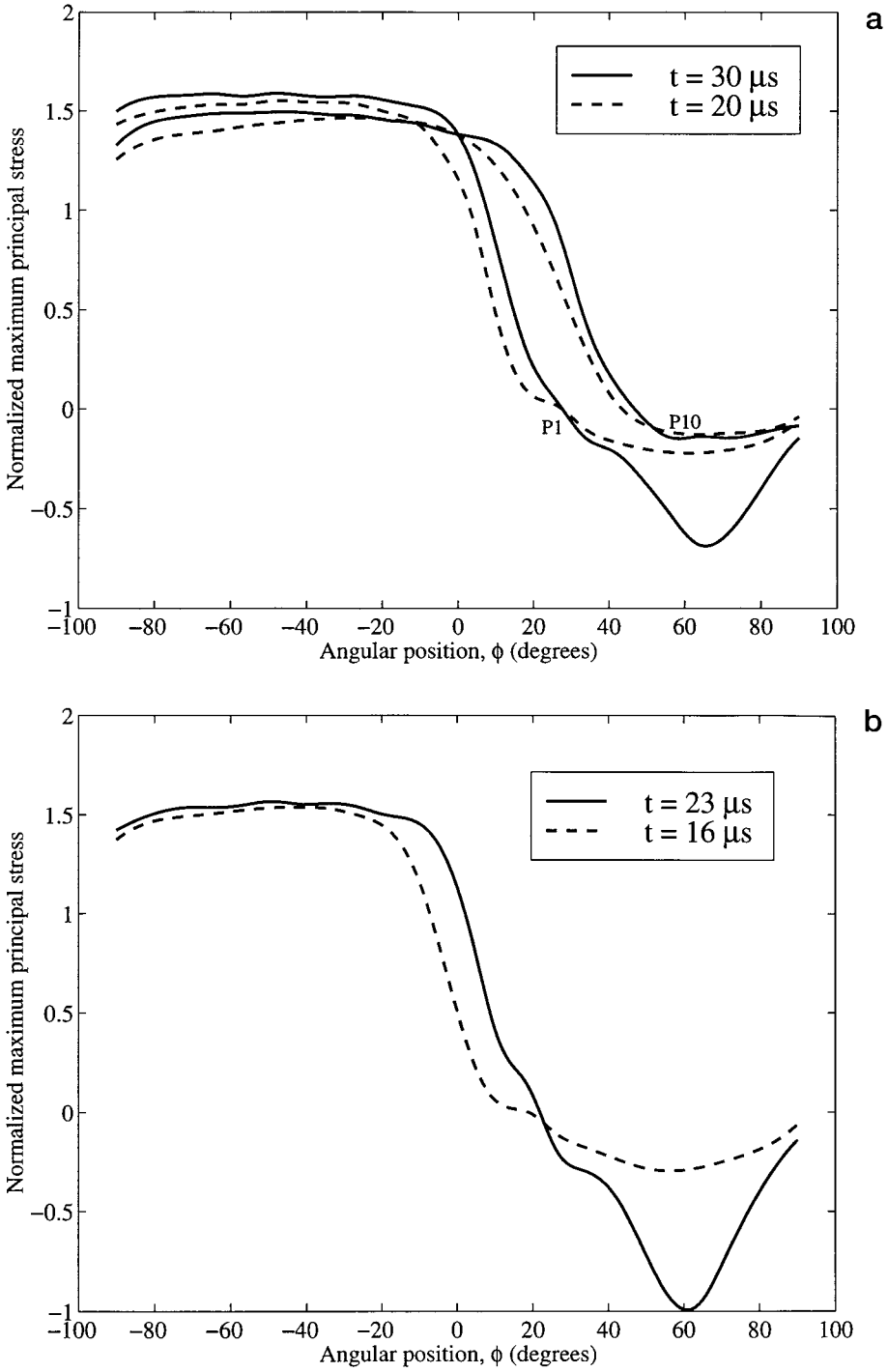

Figure 10. The normalized maximum principal stress vs. the angular position in the reference configuration of elements around the notch surface; (a) 3-D simulation, (b) 2-D simulation.

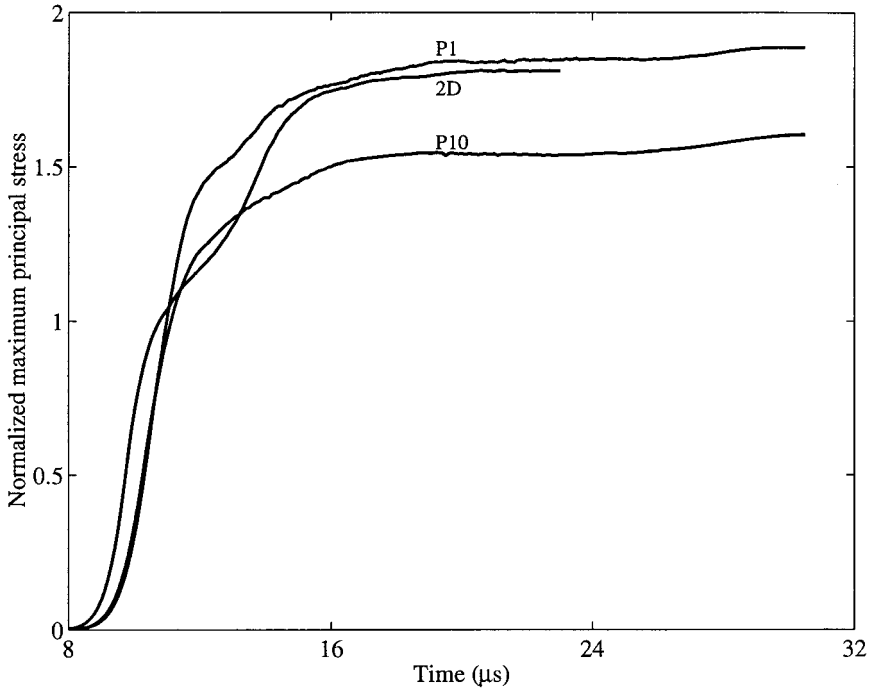

Figure 10. Time-history of the maximum principal stress at material points (0.37 mm, −63.75°, h/40) and (0.37 mm, −63.75°, 19 h/40) in the 3-D simulation and at the material point (0.37 mm, −63.75°) for the 2-D simulation.

for the 3-D simulations. Thus a shear band initiates sooner, as conjectured above, in the steel with $A = 2.36$ GPa as compared to that in the steel with $A = 0.792$ GPa. For all practical purposes, it initiates simultaneously in layers 1 through 8 in the stronger steel. The effective plastic strain in the shear banded elements in layers 1, 8 and 10 at $t = 14$ μs equaled 0.22, 0.2 and 0.13, respectively, and that in the shear banded element in the 2-D simulations was 0.32; the corresponding values at $t = 16$ μs were found to be 0.41, 0.33 and 0.19 for the 3-D simulations and 0.62 in the 2-D analysis of the problem. Hence, as expected, the effective plastic strain at the initiation of a shear band is lower in the stronger steel. However, the temperature rise in the two steels at the time of initiation of a shear band is essentially the same. This agrees with Batra and Kim's (1992) observation that the homologous temperature at the instant of the initiation of a shear band is nearly the same in the twelve materials they studied. The time-history of the evolution of different components of the Cauchy stress tensor in the shear banded elements revealed that nearly plane strain state of deformation prevailed on the midplane of the plate, the maximum value of $|\sigma_{23}|$ equaled 0.8 times the maximum value of $|\sigma_{12}|$ in the steel with $A = 0.792$ GPa, but the ratio of the two quantities in the stronger steel was 0.2. Note that $|\sigma_{12}|_{\max}$ and $|\sigma_{23}|_{\max}$ do not occur simultaneously in an element. Thus, there is less K_{III} component of deformation in the steel with $A = 2.36$ GPa as compared to that in the steel with $A = 0.792$ GPa.

3.2. Plate made of a C-300 steel

Mason et al. (1994) and Zhou et al. (1996a) tested prenotched plates made of a C-300 maraging steel and have given the effective stress vs. the effective strain curves for the material

of the plate. Zhou et al. (1996b) modeled the strain and strain-rate hardening of the material by power law type relations and the thermal softening by an exponential function. Batra and Gummalla (2000) have shown that strain-rate hardening plays a less noticeable role in the deformations at the notch-tip of a prenotched plate. Strain hardening in the Johnson–Cook model is essentially of the power law type. Thus in order to model the thermomechanical response of the C-300 maraging steel, we changed Equation (6) to

$$\sigma_m = (A + B(\epsilon_p)^n)\left(1 + C\ln\left(\frac{\dot{\epsilon}_p}{\dot{\epsilon}_0}\right)\right)(1 - \delta\exp((\theta - \theta_0)/\kappa - 1)). \tag{16}$$

Values of material parameters appearing in (18) obtained by fitting curves to the data computed from Zhou et al. (1996b) relation are (e.g., see Batra and Stevens, 1998)

$$A = 2\text{ GPa}, \quad B = 94.5\text{ MPa}, \quad n = 0.2, \quad C = 0.0165, \quad \theta_0 = 293\text{ K},$$

$$\dot{\epsilon}_0 = 1.3 \times 10^{-13}/\text{s}, \quad \kappa = 500\text{ K}, \quad \delta = 0.08. \tag{17}$$

Normalized effective stress vs. effective plastic strain curves at $\dot{\epsilon}_p = 10^5/\text{s}$ for the C-300 steel characterized by Equations (16) and (17) and also when κ is changed to 800 K are depicted in Fig. 2. This material exhibits very high strain-rate hardening as evidenced by the rather large value, 1.3, of the normalized effective stress at an infinitesimal value of the effective plastic strain. The effective stress begins to drop after a very small value of the effective plastic strain. For $\kappa = 800$ K and $\epsilon_p \geqslant 0.03$, the normalized effective stress vs. the effective plastic strain curve is essentially parallel to that for the high strength steel studied in Section 3.1. As expected, the C-300 steel with $\kappa = 500$ K exhibits more softening than the C-300 steel with $\kappa = 800$ K.

The time-histories of the evolution of the effective stress at the notch-tip indicate that, according to definition (i), a shear band initiates on the midplane of the plate at $t = 12$ μs and 12.8 μs for $\kappa = 500$ K and 800 K, respectively; the corresponding values for the 2-D simulations are 11.25 μs and 12.2 μs. Thus the shear band initiates a little sooner in the C-300 steel as compared to that in the high strength steel of Section 3.1. Not only the shear band initiates earlier in the C-300 steel with $\kappa = 500$ K as compared to that in the C-300 steel with $\kappa = 800$ K, its speed in the thickness direction is higher by a factor of about 3. The fringe plots in layers 1, 8 and 10 of the effective plastic strain for the C-300 steel with $\kappa = 800$ K are quite similar to those obtained in the same layers for the high strength steel of Section 3.1. However, for the C-300 steel with $\kappa = 500$ K the fringe plots of the effective plastic strain in layer 10 indicate that the material in the thickness direction is more severely deformed than that in the steel with $\kappa = 800$ K. For the 2-D simulations, the shear band initiating from a point on the lower surface of the notch-tip has two lobes for both values of κ. Whereas in the steel with $\kappa = 800$ K, the effective plastic strains at points within the two lobes are nearly the same, for the steel with $\kappa = 500$ K, the material in the lobe inclined at 135° clockwise from the axis of the notch has a higher value of the effective plastic strain than that in the material of the lobe which is essentially parallel to the axis of the notch. The time-histories of the normalized maximum principal tensile stress at the point (0.37 mm, $-63.75°$, $h/40$) indicate that its maximum value equals 1.85 and 1.81 for the two steels with $\kappa = 800$ K and 500 K, respectively. Thus the enhanced thermal softening has virtually no effect on the maximum value of the tensile principal stress.

4. Conclusions

We have studied three-dimensional thermomechanical deformations of a prenotched plate impacted on the side by a cylindrical projectile of diameter equal to the distance between the two notches in the plate. The diameter of the projectile equals nearly eight times the thickness of the plate. Both the projectile and the plate are made of the same material which exhibits strain and strain-rate hardening and thermal softening. The contact surface between the projectile and the plate is taken to be smooth. The strength of the steel is varied by changing the value of its yield stress in a quasistatic simple tension or compression test.

It is found that the maximum velocity in the impact direction imparted to plate particles that contact the projectile equals 90% of the initial speed of the projectile. The state of deformation near the midsurface of the plate closely resembles that given by the assumption of plane strain state of deformation in the plate but significantly differs from that on the front surface of the plate. Neither the assumption of plane strain nor that of plane stress seems to be supported by the results computed from the 3-D simulations. Whereas the shear band on the midsurface of the plate and initiating from a point on the lower surface of the notch-tip has two lobes – one nearly parallel to the axis of the notch and the other at about 135° clockwise from it, that on the front face of the plate has only one lobe aligned parallel to the axis of the notch. The temperature rise at the material point where the shear band first initiates is 190°C at the instant of the initiation of the shear band. Whereas deformations on the midplane of the plate are K_{II} dominated, those on the front face of the plate have a significant K_{III} component for a mild steel plate but a small K_{III} component for a plate made of a high strength steel. The shear band forms sooner and at a lower value of the effective plastic strain in the high strength steel plate as compared to that in the low strength steel plate. Also, the 2-D simulations predict earlier initiation of the shear band as compared to the 3-D simulations.

Acknowledgement

This work was supported by the ONR grant N00014-98-0300 to Virginia Polytechnic Institute and State University with Dr Y.D.S. Rajapakse as the program manager.

References

Batra, R. C. and Adulla, C. (1995). Effect of prior quasistatic loading on the initiation and growth of dynamic adiabatic shear bands. *Archives of Mechanics* **47**, 485–498.

Batra, R. C. and Gummalla, R. R. (2000). Effect of material and geometric parameters on deformations near the notch-tip of a dynamically loaded prenotched plate. *International Journal of Fracture* **101**, 99–140.

Batra, R. C. and Jayachandran, R. (1992). Effect of constitutive models on steady state axisymmetric deformations of thermoelastic-viscoplastic targets. *Internatioanl Journal of Impact Engineering* **12**, 209–226.

Batra, R. C. and Kim, K.H. (1990). Effect of viscoplastic flow rules on the initiation and growth of shear bands at high strain rates. *Journal of the Mechanics and Physics of Solids* **38**, 859–874.

Batra, R. C. and Kim, C.H.. (1991). Effect of thermal conductivity on the initiation, growth and bandwidth of adiabatic shear bands. *International Journal of Engineering Science* **29**, 949–960.

Batra, R. C. and Kim, C.H. (1992). Analysis of shear bands in twelve materials. *International Journal of Plasticity* **8**, 425–452.

Batra, R. C. and Nechitailo, N. V. (1997). Analysis of failure modes in impulsively loaded pre-notched plates. *International Journal of Plasticity* **13**, 291–308.

Batra, R. C. and Rattazzi, D. (1997). Adiabatic shear banding in a thick-walled steel tube. *Computational Mechanics* **5**, 442–426.

Batra, R. C. and Stevens, J. B. (1998). Adiabatic shear bands in axisymmetric impact and penetration problems. *Computer Methods in Applied Mechanics and Engineering* **151**, 325–342.

Batra, R. C., Rajapakse, Y. D. S. and Rosakis, A. J. (eds.). (2000) Failure mode transitions under dynamic loading. *International Journal of Fracture* **101**, 1–180.

Batra, R. C. and Chen, L. (2000). Effect of viscoplastic relations on the instability strain, shear band initiation strain, the strain corresponding to the minimum shear band spacing, and the band width in a thermoviscoplastic material (pending publication).

Chen, L. and Batra, R. C. (1998). Analysis of material instability at an impact loaded crack tip, *Theoretical and Applied Fracture Mechanics* **29**, 213–217.

Curran, D. R., Seaman, L. and Shockey, D. A. (1987). Dynamic failure of solids. *Physics Reports* **147**, 253–388.

Dowling, N. E. (1993). *Mechanical Behavior of Materials*, Prentice Hall, New York.

Johnson, G. R. and Cook, W. H. (1983). A constitutive model and data for metals subjected to large strains, high strain rates, and temperatures. *Proceeding 7th International Symposium Ballistics*, The Hague, The Netherlands, 1–7.

Kalthoff, J. F. (1987). Shadow optical analysis of dynamic shear fracture. *SPIE, Photomechanics and Speckle Metrology* **814**, 531–538.

Kalthoff, J. F. and Winkler, S. (1987). Failure mode transition at high rates of shear loading. In: *Impact Loading and Dynamic Behavior of Materials* (Edited by Chiem, C.Y., Kunze, H.D. and Meyer, L.W.) Vol. 1, 185–195.

Kalthoff, J. F. (2000). Modes of dynamic shear failure in solids. *International Journal of Fracture* **101**, 1–31.

Kim, C. H. and Batra, R.C. (1992). Effect of initial temperature on the initiation and growth of shear bands in a plain carbon-steel, *International Journal of Nonlinear Mechanics* **27**, 279–291.

Klepaczko, J. R., Lipinski, P. and Molinari, A. (1987). An analysis of the thermoplastic catastrophic shear in some metals, in Chiem, C. Y., Junze, H. D. and Meyer, L. W. (eds.), *Impact Loading and Dynamic Behavior of Materials*, Verlag, **1**, 695–704.

Lee, Y. J. and Freund, L.B. (1990). Fracture initiation due to asymmetric impact loading of an edge cracked plate. *Journal of Applied Mechanics* **57**, 104–111.

Marchand, A. and Duffy, J. (1988). An experimental study of the formation process of adiabatic shear bands in a structural steel. *Journal of the Mechanics and Physics of Solids* **36**, 251–283.

Mason, J. J., Rosakis, A.J. and Ravichandran, G. (1994). Full field measurements of the dynamic deformation field around a growing adiabatic shear band at the tip of a dynamically loaded crack or a notch. *Journal of the Mechanics and Physics of Solids* **42**, 1679–1697.

Mason, J. J., Zimmerman, J. A. and Roessig, K. M. (1998). The effect of ageing condition on shear localization from the tip of a notch in maraging steel. *Journal of Material Sciences* **33**, 1451–1460.

Needleman, A. and Tvergaard, V. (1995). Analysis of brittle-ductile transition under dynamic shear loading. *International Journal of Solids and Structures* **32**, 2571–2590.

Perzyna, P. (1986). Constitutive modeling for brittle dynamic fracture in dissipative solids. *Archive of Mechanics* **38**, 725–738.

Ravi-chandar, K., Lu, J., Yang, B. and Zhu, Z. (2000). Failure mode transitions in polymers under high strain loading. *International Journal of Fracture* **101**, 33–72.

Ritchie, R. O., Knott, J.F. and Rice, J. R. (1973). On the relationship between critical tensile stress and fracture toughness in mild steel. *Journal of the Mechanics and Physics of Solids* **21**, 395–410.

Roessig, K. M. and Mason, J. J. (1998). Adiabatic shear localization in the impact of edge-notched specimens. *Experimental Mechanics* **38**, 196–203.

Taylor, G. I. and Quinney (1934). The latent energy remaining in a metal after cold working. *Proceeding of the Royal Society* **A413**, 307.

Tvergaard, V. and Needleman, A. (1984). Analysis of the cup-cone fracture in a round tensile bar. *Acta Metallurgica* **32**, 157–169.

Vandergiessen, E., Vanderburg, M. W. D., Needleman, A. and Tvergaard, V. (1995). Void growth due to creep and grain-boundary diffusion at high triaxialities. *Journal of the Mechanics and Physics of Solids* **43**, 123–165.

Whirley, R. C. and Hallquist, J. O. (1991). DYNA3D User's Manual (A nonlinear explicit three-dimensional finite element code for solid and structural mechanics), UCRL-MA-107254, University of California, Lawrence Livermore National Laboratory.

Zhou, M., Rosakis, A. J. and Ravichandran, G. (1996a). Dynamically propagating shear bands in prenotched plates: I – experimental investigations of temperature signatures and propagation speed. *Journal of the Mechanics and Physics of Solids* **44**, 981–1006.

Zhou, M., Ravichandran, G. and Rosakis, A. J. (1996b). Dynamically propagating shear bands in prenotched plates: II – finite element simulations. *Journal of the Mechanics and Physics of Solids* **44**, 1007–1032.